

UKAEA-CCFE-PR(22)05

D. Brunetti, C. J. Ham, J. P. Graves, E. Lazzaro, S.  
Nowak, A. Mariani, C. Wahlberg, W. A. Cooper, E. R.  
Solano, S. Saarelma, L. Frassinetti, M. Fontana, A.  
Kleiner, G. Bustos Ramirez, E. Viezzer, JET  
contributors

# **Understanding JET-C quiescent phases with edge harmonic magnetohydrodynamic activity and comparison with ITER-like wall conditioning**

Enquiries about copyright and reproduction should in the first instance be addressed to the UKAEA Publications Officer, Culham Science Centre, Building K1/O/83 Abingdon, Oxfordshire, OX14 3DB, UK. The United Kingdom Atomic Energy Authority is the copyright holder.

The contents of this document and all other UKAEA Preprints, Reports and Conference Papers are available to view online free at [scientific-publications.ukaea.uk/](https://scientific-publications.ukaea.uk/)

# **Understanding JET-C quiescent phases with edge harmonic magnetohydrodynamic activity and comparison with ITER-like wall conditioning**

D. Brunetti, C. J. Ham, J. P. Graves, E. Lazzaro, S. Nowak, A. Mariani, C. Wahlberg, W. A. Cooper, E. R. Solano, S. Saarelma, L. Frassinetti, M. Fontana, A. Kleiner, G. Bustos Ramirez, E. Viezzer,  
JET contributors



# Understanding JET-C quiescent phases with edge harmonic magnetohydrodynamic activity and comparison with behaviour under ITER-like wall conditioning

D. Brunetti,<sup>1,\*</sup> C. J. Ham,<sup>1</sup> J. P. Graves,<sup>2</sup> E. Lazzaro,<sup>3</sup> S. Nowak,<sup>3</sup> A. Mariani,<sup>3</sup>  
C. Wahlberg,<sup>4</sup> W. A. Cooper,<sup>5</sup> E. R. Solano,<sup>6</sup> S. Saarelma,<sup>1</sup> L. Frassinetti,<sup>7</sup> M.  
Fontana,<sup>2</sup> A. Kleiner,<sup>8</sup> G. Bustos Ramirez,<sup>2</sup> E. Viezzer,<sup>9</sup> and JET contributors<sup>†</sup>

<sup>1</sup>UKAEA-CCFE, Culham Science Centre, Abingdon, Oxon, OX14 3DB, United Kingdom

<sup>2</sup>École Polytechnique Fédérale de Lausanne (EPFL),

Swiss Plasma Center (SPC), CH-1015 Lausanne, Switzerland

<sup>3</sup>Istituto per la Scienza e Tecnologia dei Plasmi CNR, Via R. Cozzi 53, 20125 Milan, Italy

<sup>4</sup>Department of Physics and Astronomy, P.O. Box 516, Uppsala University, SE-751 20 Uppsala, Sweden

<sup>5</sup>Swiss Alps Fusion Energy (SAFE), CH-1864 Vers l'Eglise, Switzerland

<sup>6</sup>Laboratorio Nacional de Fusión, CIEMAT, Madrid, Spain

<sup>7</sup>Division of Fusion Plasma Physics, KTH Royal Institute of Technology, Stockholm, SE, Sweden

<sup>8</sup>Princeton Plasma Physics Laboratory, Princeton University, Princeton, New Jersey 08543, USA

<sup>9</sup>Department of Atomic, Molecular and Nuclear Physics,

University of Seville, Avda. Reina Mercedes, 41012 Seville, Spain

(Dated: September 5, 2021)

The analysis of ELM-free (quiescent) H-mode discharges exhibiting edge harmonic magnetohydrodynamic activity in the JET-Carbon wall machine is presented. It is observed that the otherwise quiescent with multiple- $n$  harmonic oscillations are sustained until a threshold in pedestal electron density and collisionality is crossed. The macroscopic pedestal parameters associated with the quiescent phase are compared with those of a database of JET-ELMy discharges with both carbon and ITER-like wall. This comparison provides the identification of the existence regions in the relevant pedestal and global plasma parameters for edge harmonic oscillations (EHOs) in JET plasmas. Quiescent scenarios operate at the very boundaries of the parameter space scanned by the database (both C and ILW), although improved pedestal performances could be observed in more recent JET-ILW pulses.

## I. INTRODUCTION

The most promising scenarios for achieving efficient controlled thermonuclear fusion in tokamak machines are the so called high-confinement (H-mode) regimes. Such scenarios show long energy confinement times and are typically characterised by the presence of sharp and narrow plasma edge pedestals, both in mass density and temperature. Unfortunately, the associated strong radial gradients favour the appearance of short wavelength magnetohydrodynamic (MHD) perturbations called Edge Localised Modes (ELMs) [1]. These sudden and violent events are associated with rapid energy and particle expulsions which deposit intolerable heat loads on plasma facing components. In addition to severe plasma contamination, ELMs can significantly reduce machine lifetime. Therefore, it is of crucial interest to attain high-performance scenarios without the deleterious presence of ELMs [1].

One of the most promising intrinsically ELM-free regimes is the so called quiescent H-mode (QH-mode). In this regime, which shares with the standard H-mode

large edge pressure gradients and long energy confinement times, ELMs are avoided and replaced by continuous low- $n$  mild MHD perturbations, and the associated peak energy and heat loads on the plasma facing materials are significantly lower compared to ELMy regimes. These Edge Harmonic Oscillations (EHOs) are well localised within the edge region of large gradients (pedestal) and feature multiple  $n$  toroidal harmonics with a rather long lifetime, of the order of 1s [2]. EHOs have been observed in DIII-D, ASDEX-U, JT60 [3–6], and JET [7]. In Ref. [7] such oscillations are called Outer Modes. Since the MHD dynamics described in Refs. [3, 4] and Ref.[7] have the same characteristics, for the sake of clarity, hereafter we will refer to such oscillations as EHOs<sup>1</sup>. As observed in Ref. [7], EHOs have several common features with the low- $n$  type-I ELM precursors studied in Ref. [10].

It is observed that EHOs in JET are prone to develop in the early phase of the discharge, during the density ramp when ion and electron temperatures reach their highest values at the pedestal top. It is also observed that above a critical value of the pedestal density ( $\sim 5 \times 10^{19} m^{-3}$ ) the quiescent phase with EHOs

---

\* Electronic address: [daniele.brunetti@ukaea.com](mailto:daniele.brunetti@ukaea.com)

<sup>†</sup> See the author list of ‘Overview of JET results for optimising ITER operation’ by J. Mailloux et al. to be published in Nuclear Fusion Special issue: Overview and Summary Papers from the 28th Fusion Energy Conference (Nice, France, 10-15 May 2021)

---

<sup>1</sup> Historically, Outer Modes refer to low- $n$  (mainly  $n = 1$ ) MHD oscillations with frequencies  $\sim 10kHz$  observed typically within the outer 20% of the plasma [8, 9] (broader compared to EHOs). In [9], Outer Modes refer to current driven external kinks.

abruptly ends and ELMs appear. We point out that quiescent regimes in DIII-D, ASDEX-U and JT60-U experiments [3–6] usually operate with lower values of the pedestal top density compared with JET, typically three or four times smaller. Although for some discharges EHOs can re-emerge after an ELM crash, the quiescent phase is not usually recovered after the first ELM is triggered.

Thus, the aim of this paper is to detail and characterise the existence conditions for EHOs in JET, in order to determine the pedestal features required to guarantee the accessibility to quiescent regimes with EHOs, and potentially in machines with a metallic wall. These existence conditions are assessed by comparing global and pedestal parameters, namely electron  $\beta$ , collisionality,  $q_{95}$  and triangularity, of quiescent with EHOs (Q-EHO) shots with the ones extracted from a carbon (C) and ITER-like wall (ILW) EUROfusion pedestal database of ELMy discharges [11]. It is found that the operational regime of Q-EHO plasmas identified by the parameters given above, lies typically at the very boundaries of this ELMy discharges database. This holds in particular for ILW plasmas where the electron temperature, which plays a crucial role, is significantly smaller compared to carbon wall discharges. We finally point out that some indications of brief edge coherent activity have been observed in recent hybrid JET-ILW shots with high pedestal performance. Although these oscillations have been observed transiently, efforts are now focussed on steadily sustaining this behaviour in metal machines [12].

Thus, the paper is organised as follows: In section II we describe the JET-C experimental set-up and the typical features of the EHOs which are observed during the quiescent phase. In section III we analyse a database of JET discharges with a carbon and ITER-like wall which do not exhibit EHO activity, by inspecting the associated physical global and pedestal parameters (e.g. collisionality, temperature, etc.). These parameters are then compared with the ones observed in the Q-EHO JET-C pulses analysed in section II. Finally, a discussion of the results and concluding remarks are given in section IV

## II. JET-C QUIESCENT DISCHARGES WITH EHO ACTIVITY

As a matter of notation, we indicate the electron density with  $n_e$  while ion and electron temperatures are denoted by  $T_i$  and  $T_e$  respectively. Here  $q$  is the safety factor and  $B_t$  the vacuum toroidal field at the plasma geometric centre.

We analyse a set of four JET-C discharges showing a quiescent ELM-free phase in which coherent edge harmonic oscillations are observed. These shots are listed in Table I, where the macroscopic global plasma parameters of interest for the present study are also reported. Although additional quiescent discharges having similar features with rather strong indications of the presence of

EHOs have been identified, we chose these four particular shots as the best representatives. This is because of i) relatively long quiescent phase duration, and ii) diagnostic signal clarity, i.e. most of the EHOs footprints, needed for a unique mode identification, are clearly visible on all the relevant diagnostics.

The discharges listed in Table I have similar plasma shaping, being characterised by high values of upper and lower triangularity ( $\sim 0.4$ ) with a moderate elongation  $\sim 1.7$ . Error Field Correction Coils (EFCC) for ELM control were employed in discharges #78012 and #78014 with the coil current ramp taking place between  $t = 14s$  and  $t = 14.1s$  and reaching values up to  $\pm 0.5kA$  and  $\pm 1kA$  respectively (the plus/minus sign refers to 1-5/3-7 octants). For each discharge, the time window for the later analysis is chosen to extend from  $t_1$  to  $t_2$ , subdivided into 40 time slices, in which a transition from quiescent to ELMy behaviour is observed. The initial time  $t_1$  is chosen to correspond approximately to the EHO appearance, whereas at time  $t_2$  the plasma is deeply into the ELMy phase. After  $t = t_{ELM}$ , the quiescent phase is never recovered and the plasma enters the ELMy regime. We note that in discharge #78012 a first quiescent phase lasts until  $t \approx 14.3s$  when an ELM occurs and the EHO is lost; after this ELM event, the EHO is recovered at  $t \approx 14.45s$  and lasts until  $t_{ELM}$ . In #79455 instead, the EHO disappears spontaneously at  $t \approx 14.64s$ , whereas the quiescent state persists until  $t = t_{ELM}$ . The ICRH heating is switched on only at the very end of each pulse, so that we regard these shots as Ohmically and NBI heated.

All pulses in Table I exhibit similar behaviour, in which the electron temperature increases all across the plasma column during the early phase when the NBI is switched on, and whose power is steadily maintained for the whole discharge (cf. Fig. 7). At the same time, the plasma density is ramped up, reaching the stationary core value  $> 7 - 8 \times 10^{19} m^{-3}$ . The value of the pedestal density rises accordingly, as shown in figure 1 from high resolution Thomson scattering (HRTS) measurements. Details on the definition of pedestal quantities, e.g. height and width, are detailed in Ref. [13]. The density rise is accompanied by an increase of  $Z_{eff}$  which ranges approximately from 1.8 to 2 during the quiescent phase, whereas in the ELMy phase it can reach values up to 2.5. Since EHOs are observed in low pedestal collisionality regimes [4, 14] and because  $\nu_{e*} \propto n_e Z_{eff}$  [15, 16], plasmas with a higher percentage of impurities may require smaller pedestal densities in order to keep the pedestal electron collisionality sufficiently small, as pointed out in [5].

As the mass density is ramped up, the toroidal rotation  $v_{tor}$ , obtained from charge exchange measurements which are also used to infer the ion temperature profile, is observed to reduce as expected (see figure 2). During this phase  $\beta_N$  remains approximately constant. Note that in JET the NBI injection is co-current [17]. In the time window indicated in Table I, ion and electron temperatures decrease, with  $T_i$  having smaller gradients in

Shot#	$B_t$ [T]	$I_p$ [MA]	NBI [MW]	$\beta_N$	$t_1$ [s]	$t_2$ [s]	$t_{ELM}$ [s]	$q_{95}$
75411	2.7	2.5	15.3	1.94	14	16	15.4	3.37
78012	2.7	2.5	16.8	1.87	13.6	16	14.65	3.36
78014	2.7	2.5	16.7	1.98	13.8	16	14.23	3.38
79455	2.7	2.5	11	1.67	14	16	14.85	3.3

Table I. Macroscopic global plasma parameters for the four JET-C discharges with EHO activity. Shaping is similar in all shots. Note the  $\approx 30\%$  reduction in the injected NBI in pulse #79455. The time  $t_1$  is chosen to correspond to the appearance of the EHO, while  $t_{ELM}$  indicates the time of the ELM event after which the quiescent phase with EHOs is lost. The analysis is performed until  $t_2$  in which the plasma is deeply into the ELMING phase. Here  $\beta_N = \beta[\%]a[m]B_T[T]/I_p[MA]$  and  $q_{95}$  are the averaged value over each pulse's time window. Similar values of  $q_{95}$  were observed ASDEX-U [5].

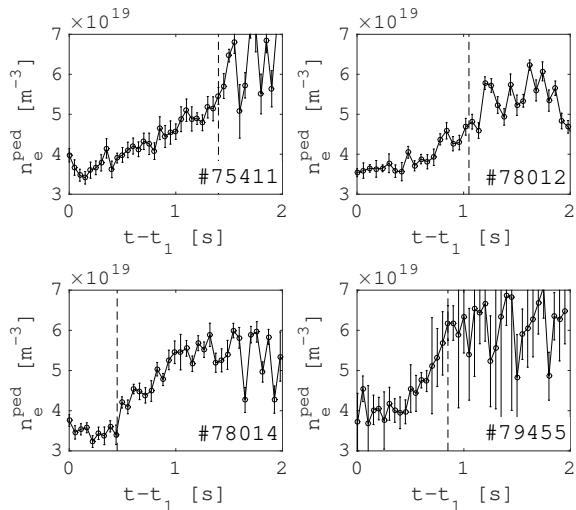


Figure 1. Evolution of the pedestal density for the discharges of Table I. A steady increase in  $n_e^{ped}$  is observed. The dashed vertical lines in each plot indicate the appearance of the ELM after which the Q-EHO phase is lost. Note the large errorbars in the pedestal density value after the first ELM appearance in shot #79455 (errorbars are obtained by a weighted fit of HRTS data).

the pedestal compared with  $T_e$ . We observed that  $T_i$  and  $v_{tor}$  have similar radial dependencies. We point out that during the quiescent phase the ion temperature at the pedestal top is slightly larger on average compared with the electron temperature, the former taking values about  $2keV$  whereas the latter is  $\sim 1.4 - 1.5keV$  at the EHO onset. After the appearance of the first ELM, we observe  $T_i^{ped} \approx T_e^{ped}$ . As a matter of notation, hereinafter the superscript *ped* will indicate that the associated physical quantity is evaluated at the pedestal top.

Very rich MHD dynamical behaviour, which is similar in all the four shots of Table I, is observed during the early NBI heating phase as clearly shown in figure 3 (note the short lived multiple harmonics appearing before ELMs from 14.3 to 14.5s). During the density ramp-up,

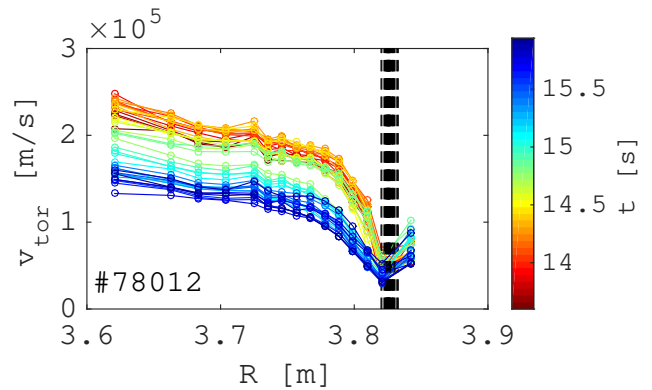


Figure 2. Time evolution of the toroidal (C) rotation profile for discharge #78012 from charge exchange measurements in the time window indicated in Table I (early times in red, later ones in dark blue). Error bars are not shown for the sake of visual clarity. A steady decrease of the core rotation frequency is observed. Note that the separatrix position is allowed to vary within the region delimited by the dashed vertical line.

when the electron temperature is the highest, a clear signature of multiple  $n$  harmonics all equally spaced in the frequency domain appear on the magnetic diagnostics. In order to assess the radial location of these MHD modes, and therefore identify their EHO-like nature, in analogy with Refs. [5, 14] we compare magnetic with electron cyclotron emission (ECE) signals. The EHO is uniquely identified by matching the rotation frequencies of the various harmonics measured by the magnetic and ECE diagnostics. The ECE channels distribution and location in the major radius of the outer midplane is given in figure 4. Note that for all the shots listed above, channels 54 and 66 are usually associated with pedestal measurements (odd number channels were not available).

A typical spectrogram of an ECE near-pedestal signals (channel 66 of Fig. 4) is shown in figure 5. The electron temperature fluctuation with the many- $n$  harmonic structure displayed in figure 3 is clearly recognisable in the edge ECE channel 66. It is found that the ECE signal does not propagate further beyond the pedestal shoulder.

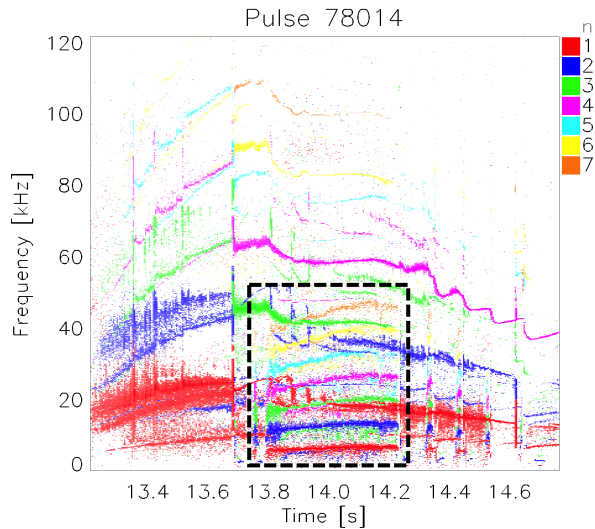


Figure 3. MHD mode analysis of the early phase of discharge #78014. A MHD activity with multiple harmonics up to  $n = 7$  is observed from  $t = 13.8$ s to  $t = 14.2$ s (highlighted in the dashed box). Brief coherent MHD bursts localised in the pedestal region appear before ELM crashes at 14.35, 14.45 and 14.53s, resembling the type-I ELM precursor activity discussed in Ref. [10].

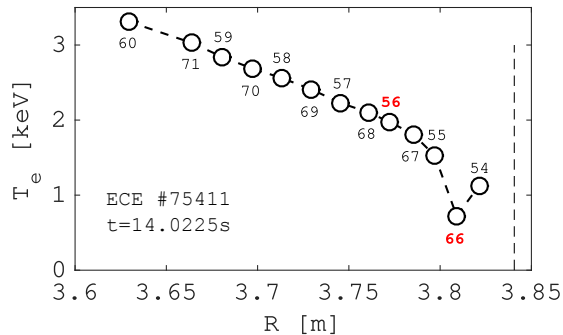


Figure 4. Temperature profiles of shot #75411 showing the major radius location of the ECE lines of sight. Note that in all discharges listed in Table I, the pedestal ECE emission is, with a good approximation, associated with channel 66 (highlighted in red). Channel 56 is the nearest-non pedestal channel, so that it is always inspected to check the edge mode localisation. It is important to point out that even channels only are associated with the fast ECE data acquisition. The separatrix position is denoted by the dashed vertical line.

Indeed, as clearly shown in figure 6, the ECE trace of the EHO is not visible inside channel 56 which is the first available channel in the core region outside the pedestal. Similar behaviour, which also resembles the dynamics of low- $n$  ELM precursors studied in Ref. [10], has been reported in DIII-D and JT60-U experiments [6, 18]. This provides confidence on the pedestal radial localisation of the EHO which must indeed be extremely narrow.

We note that the ELM appearance does not necessarily

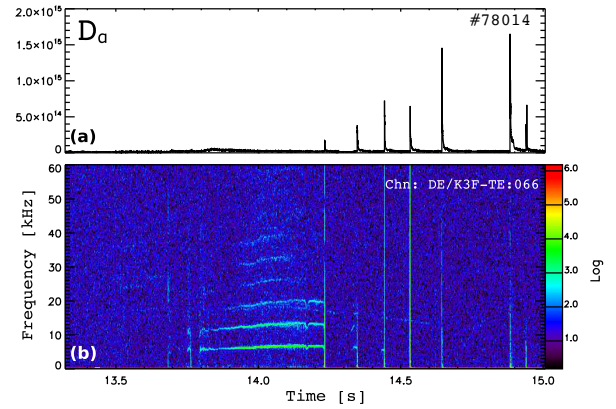


Figure 5. Time trace of the  $D_\alpha$  outer divertor signal (a) and the ECE emission channel 66 (b) for JET discharge number #78014. The EHO lasts for approximately 400ms from  $t = 13.8$ s to  $t = 14.2$ s. The ECE signals (colourbar in log scale) have to be compared with the magnetics shown in Fig 3.

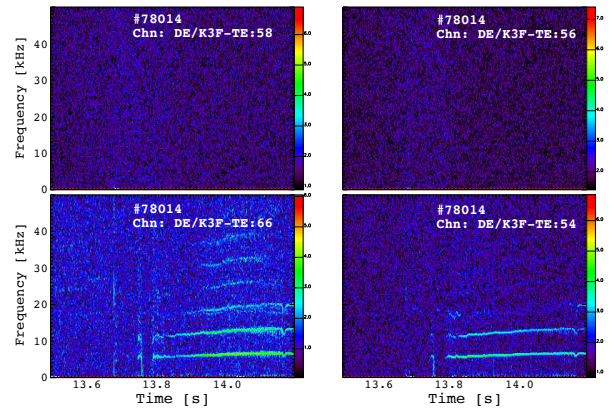


Figure 6. Spectrogram of the ECE emission (colourbar in log scale) for channels 54, 56, 58 and 66 (cf. Fig. 4) for shot #78014.

imply a complete loss of the quiescent phase. Indeed, as discussed above, in discharge #78012 the Q-EHO phase is recovered after an ELM event and lasts for further  $\sim 0.23$ s. Also, it is worth pointing out that there were no active EFCCs in discharges #75411 and #79455. Moreover, by noticing that the (dis-)appearance of the EHOs in shots #78012 and #78014 occurs for times well (after)-before the EFCCs switch on, we conjecture that EHO dynamics are not affected by external magnetic perturbations, i.e. the mode has to be driven purely by internal mechanisms.

We now argue that the toroidal rotation gradient is not a key ingredient for the appearance of EHOs. This is because we observe that the toroidal rotation frequency at the pedestal top drops *after* the appearance of the first ELM (cf. figure 7). Moreover, although a connection between toroidal (carbon) rotation shear and Q-EHO phase was established in Ref. [7], DIII-D results of Ref. [19] show that the accessibility of the quiescent phase is al-

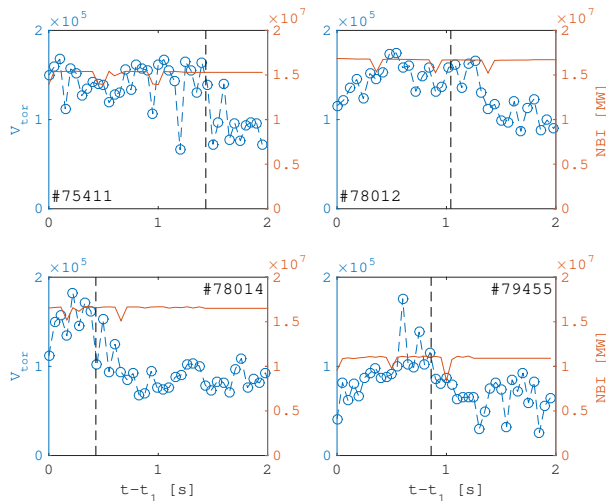


Figure 7. Toroidal rotation at the pedestal top (computed by averaging density and electron temperature pedestal positions) and NBI power for the four shots of Table I. Note that, despite the steady NBI power, a drop in the rotation pedestal value occurs at the appearance of first ELM, indicated by the dashed vertical line, after which the EHO phase is lost.

most independent of the toroidal (carbon) rotation shear. In addition, figure 7 seems to suggest that EHOs exist within a broad range of pedestal rotation frequencies. It is also worth stressing that there could be a consistent difference between carbon and main-ion species rotation profiles in the pedestal region, the latter exhibiting significantly weaker gradients [20–22]. Furthermore, nonlinear MHD simulations with the JOREK code [23] found that toroidal flows have a weak effect on the destabilisation and saturation of modes which might be related to a Q-EHO phase. Interestingly, we notice that similar low- $n$  edge localised oscillations with a dominant  $n = 1$  component have been recently reported in Alcator C-Mod in low-collisionality and high pressure pedestal regimes [24]. No NBI was employed in the C-Mod experiments [24], supporting our claim that these low- $n$  edge fluctuations do not depend explicitly on plasma toroidal rotation gradient. In conclusion, the experimental evidence in JET, also supported by the results presented in Refs. [6, 19] and numerical modelling, gives us confidence that other physical effects might be more relevant for the EHO appearance.

As pointed out in Ref. [19], one of the key parameters which determine the accessibility to the quiescent phase is the edge  $E \times B$  flow shear. This flow manifests itself as a plasma rotation mainly in the poloidal direction, and its strength is proportional to the radial electric field. From the radial ion force balance equation [25], allowing for plasma shaping through elongation, we have near the edge

$$E_r \approx \sqrt{\frac{2}{1 + \kappa^2}} \left( \frac{dp_i/dR}{en_i} + \frac{a\kappa B_t}{q} \Omega_{tor} \right) - v_{pol} B_t,$$

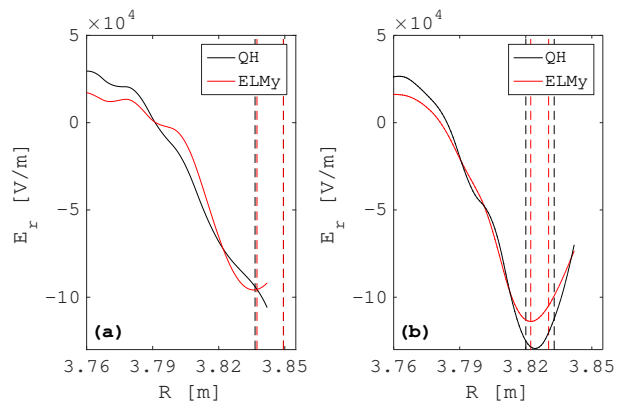


Figure 8. Radial electric field for pulses #75411 (a) and #78012 (b) during the quiescent (black, averaged over  $t_1 - t_{ELM}$ ) and ELMy (red, averaged over  $t_{ELM} - t_2$ ) phases. The separatrix position varies within the region indicated by the two vertical dashed lines (same colour meaning as for  $E_r$ ).  $E_r$  has been calculated up to  $R = 3.8425m$  for which averaged  $T_i$  data are available.

where  $p_i = n_i T_i$  with  $n_i$  the ion density,  $e$  is electric charge,  $\kappa$  the plasma elongation,  $a$  and  $R_0$  the minor and major radii respectively,  $\Omega_{tor} = v_{tor}/R$  the toroidal angular frequency and  $v_{pol}$  the poloidal velocity. The radial derivative is taken with respect the major radius on the equatorial plane (for the geometry of the beam injection and sign conventions we refer to [17, 26]). Figure 8 shows  $E_r$  averaged over the quiescent and ELMy time windows as a function of the major radius. The  $E_r$  well takes values comparable to those observed in DIII-D [18, 27] of the order of  $\sim 100kV/m$ , although no strong variations of  $E_r$  are observed when transitioning to the ELMy phase [28].

Thus, to further investigate what conditions favour the EHOs existence, we study the localisation of the discharges of Table I in  $n_e - T_e$  space. Figure 9 shows the instantaneous pedestal values of density and electron temperature during the time window  $t_1 - t_2$  for the four shots considered. We observe that the Q-EHO phase exists in the region of low-density with temperatures  $\gtrsim 1keV$ . Note that most of the high pressure values associated with an ELMy pedestal belong to pulse #78014, and these may be connected with the EHO-like bursts prior to ELMs shown in figure 3. During the discharge, the plasma evolves towards an ELMy regime which loses the EHOs.

As shown in Fig. 10-(a) and (b), the pedestal density increase is accompanied by a temperature decrease where the pedestal knee appears to shift inwards, at least for the electron temperature. This leads to an increase of the pedestal collisionality<sup>2</sup> and the EHO is lost when  $\nu_{e*} \gtrsim 0.3$  (cf. Fig. 10-c), in line with the results in DIII-D and JT60-U [29]. This is likely to be associated with vari-

<sup>2</sup> We employ the following definition for the pedestal collisional-

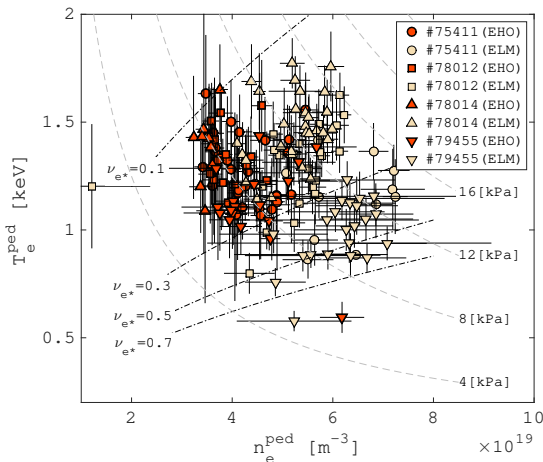


Figure 9. Scatter plot of the instantaneous pedestal values for density and electron temperature at the pedestal top for the discharges in Table I during the selected time window (we point out that the pedestal position of  $n_e$  is approximately the same of the  $T_e$  one). The red points refer to ELM-free phases with EHO activity. The constant electron pressure and collisionality level curves are also indicated. EHOs tend to cluster in high temperature-low density regions.

ations of the pedestal bootstrap contribution, and hence to a local modification the magnetic shear [15, 30–32]. Since the increase of collisionality yields a reduction of the bootstrap current which in turn increase the local shear, we conjecture that there exists a critical magnetic shear below which EHOs can develop [33]. This is indeed in accordance with recent analytic and numerical modelling [34–37] which predict unstable EHOs if the shear is weak.

It is worth noting that EHOs in DIII-D, ASDEX-U and JT60 have been observed in discharges with low pedestal density of the order of  $1 \times 10^{19} m^{-3}$  and plasma currents of  $1 MA$  [3–6], whereas JET quiescent plasmas can be sustained up to fairly large values of pedestal density ( $n_{e,crit}^{ped} \sim 5 \times 10^{19} m^{-3}$ , cf. Fig. 1). Although most of JET pulses operate at higher plasma current, which is associated with a smaller  $q_{95}$ , this does not fully explain

ity [15]

$$\nu_{e*} = 6.921 \times 10^{-18} \frac{q_{95} R_0 n_e Z_{eff} \ln \Lambda_e}{T_e^2 \epsilon^{3/2}},$$

where  $R_0$  is the major radius with  $n_e$ ,  $T_e$  and the Coulomb logarithm  $\ln \Lambda_e$  evaluated at the pedestal top. Here  $\epsilon$  is an effective inverse aspect ratio defined by

$$\epsilon = \frac{a}{R_0} \sqrt{\frac{1 + \kappa^2}{2}},$$

with  $a$  the minor radius on the low field side part of the equatorial plane and  $\kappa$  the plasma elongation (i.e.  $R = R_0 + r \cos \theta + \dots$  and  $Z = \kappa r \sin \theta + \dots$ ).

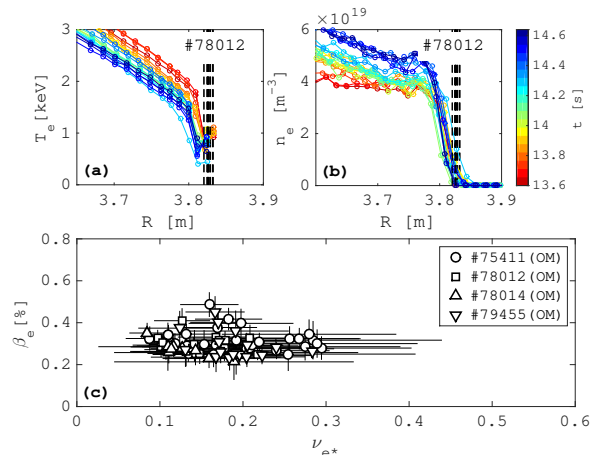


Figure 10. Electron temperature (panel (a), data from ECE) and density (panel (b), from HRTS) profiles of discharge #78012 for the time window  $t_1 - t_{ELM}$  of Table I (early times in red, later ones in dark blue). The separatrix position varies within the region identified by the vertical dashed lines. Note that for this discharge,  $T_e$  values from ECE are higher than the ones recorded by the HRTS diagnostic, although the radial profile remains the same. In (c), the instantaneous pedestal values of  $\beta_e = 2\mu_0 p_e / B_t^2$  versus  $\nu_{e*}$  of the four discharges in Table I during the Q-EHO phase are shown (these corresponds to the red points of figure 9) with  $p_e = n_e^{ped} T_e^{ped}$ .

this behaviour as local quantities such as collisionality,  $\beta_e$ ,  $Z_{eff}$  in these regimes seem to be comparable across these machines [4, 38].

We finally note that similarities between Edge Harmonic Oscillations (or Outer Modes) and the low- $n$  ELM precursors studied in Ref. [10] have been pointed out in Ref. [7]. The latter appears as multiple  $n$  coherent oscillations localised at the plasma boundary, and were observed frequently in the so-called hot-ion H-mode regimes, in which very high ion temperatures were achieved by applying NBI heating to a low density plasma [10]. In Ref. [10], it is pointed out that these MHD dynamics have been observed also in some conventional ELMy H-mode discharges. Such low- $n$  (mainly  $n = 1$ ) precursors do not extend radially beyond the pedestal shoulder but are localised within the pedestal radii.

Having specifically identified the EHOs characteristics exhibited in carbon-wall plasmas, the aim of the next section is to scan a database for several JET-C and JET-ILW discharges [11] searching for similar plasma features observed across Q-EHO plasmas. Indeed, the final aim is to assess whether or not quiescent EHO activity is compatible with metallic wall conditioned plasmas.

### III. JET-C AND ILW ELMY DATABASE PERFORMANCE ANALYSIS

Ideally, we would like to provide an answer to the following questions: If the conditions for accessing the quiescent phase are met, and yet an ELMy behaviour is observed, are there other hidden parameters which determine the access to the ELMs/no-ELMs phase? Are those conditions achievable in JET-ILW plasmas, so that quiescent states can be reproduced in metallic machines? Thus, the aim of this section is to analyse the plasma performance of a database of JET discharges with carbon and ITER-like wall, both of whom do not exhibit quiescent edge MHD activity, and consequently assess the compatibility of their associated pedestal parameters with the ones characterising JET-C pulses with EHOs. This, therefore, would allow us to determine whether or not Q-EHO scenarios can be reproduced in metallic machines, and under which specific plasma/pedestal conditions.

The JET-C/ILW database under consideration consists of 1216 shots in high performance ELMing H-mode, divided into 360 shots with carbon wall and 856 shots with ITER-like wall [11]. Further details about this database can be found in Ref. [11]. The pedestal values of the associated physical quantities are averaged over a time window of 1 – 2s during an inter-ELM stationary phase. Contrarily to the analysis of the previous section which focussed on the discharge evolution in the early phase (cf. Fig. 1), the time window of all shots in the ELMy database is taken during the steady state flat-top. It is worth stressing that if EHOs exist during a transient phase, i.e. they are robust, they should be expected to be observed during the flat-top if the plasma conditions required for their existence are met.

In analogy with figure 9, the pedestal electron temperatures plotted versus density for the shots in the database are shown in Fig. 11. At first glance, ILW discharges tend to occupy the lower part of the  $n_e^{ped} - T_e^{ped}$  plane having on average lower temperatures, while exploring regions of similar densities. We observe that for these pulses the ion and electron temperatures have comparable values (i.e.  $T_i \sim T_e$ ). We point out that within this database high electron pressure regimes above 12kPa are not explored in ILW discharges. As a direct consequence, by inspecting the associated pedestal electron collisionality, we clearly see that ILW discharges tend to have higher  $\nu_{e*}$  values. Nevertheless, a reasonable number of ILW shots lie in a region of low to moderate collisionality at fairly high(low) electron temperature(density), where EHOs might be expected to exist.

As a first check, it is instructive to see whether the JET-C discharges in the database lie in the same region of the  $n_e^{ped} - T_e^{ped}$  parameter space of the quiescent ones studied in the previous section. Hence, the  $n_e^{ped} - T_e^{ped}$  data points of figure 11-(a) are overlaid with the ones of figure 9 in section II. This is shown in Fig. 12. It is immediate to notice that quiescent discharges occupy the re-

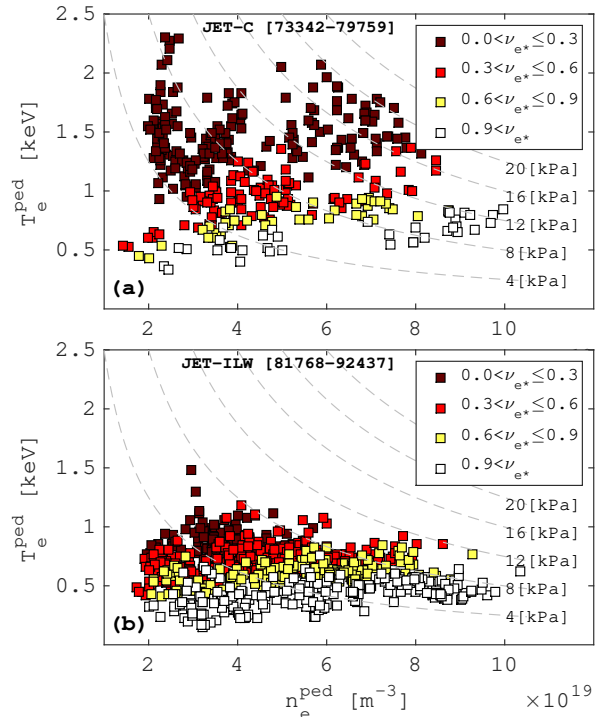


Figure 11. Scatter plot of JET carbon (a) and ILW (b) database discharges in the  $n_e^{ped} - T_e^{ped}$  parameter space (each point corresponds to a pulse in the database). The dashed lines indicate the constant electron pressure levels, while bands of different pedestal electron collisionality are indicated by the colour associated with the discharge. Note that JET-C discharges exhibit larger pedestal  $T_e$  and an associated smaller  $\nu_{e*}$  with a wider span in pedestal electron pressure.

gion of the parameter space of high temperature and low density with the electron pressure above  $\sim 7kPa$  at low collisionality ( $\nu_{e*} \lesssim 0.3$  in line with DIII-D results [4]). It should also be noted that in Fig. 12 an upper limit in pressure  $\sim 14kPa$  appears where no EHOs are observed. Beyond the small collisionality requirement, these results may suggest that quiescent EHOs phases are accessed when a threshold in the pedestal pressure is crossed. In addition, by comparing Figs. 11 and 12, the  $n_e^{ped} - T_e^{ped}$  parameter space explored by JET-ILW shots seems not to overlap with the one of the JET-C Q-EHO discharges.

However, we notice that JET-C ELMy plasmas are found in regions where EHOs are expected to exist, i.e. despite having similar pedestal characteristics with the quiescent ones. Thus, we argue that other parameters must play a key role in determining whether or not the quiescent phase is accessible. We point out that when interpreting EHOs as pedestal localised pressure driven MHD instabilities [34, 36, 39], similarly to ballooning modes and to some extent Mercier modes, it is more appropriate to compare the pedestal  $\beta$  rather than the pressure alone. This indeed is shown in figure 13, where the pedestal values of  $\beta_e$  of the carbon and ILW database

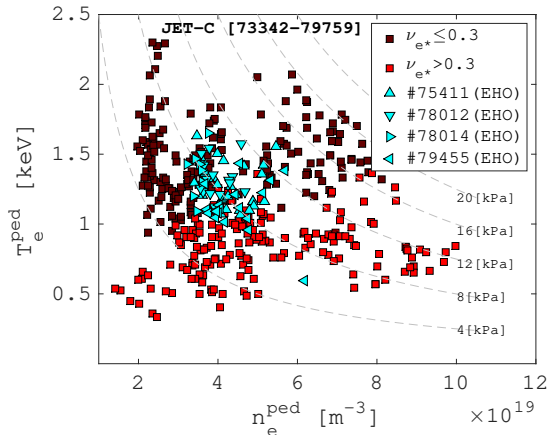


Figure 12. Plot of the JET-C points of figure 11-(a) overlaid with the  $n_e - T_e$  pedestal values of discharge of Table I during the quiescent phase with EHOs. Note how the quiescent discharges tend to cluster in the region of high  $T_e$  and low  $n_e$  with electron pressure above  $\sim 7kPa$ , though there are no EHOs for pressure larger than  $14kPa$ , regardless of  $n_e$  and  $T_e$ .

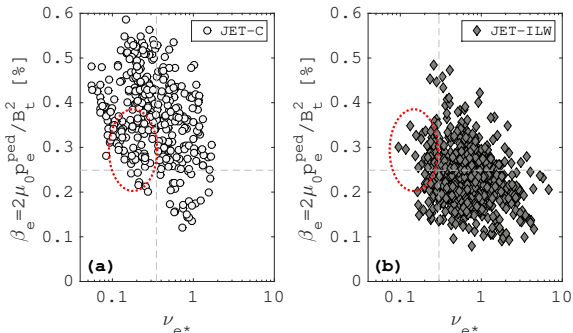


Figure 13. Scatter plot of the JET-C (a) and ILW (b) database of the pedestal values of  $\beta_e$  vs  $\nu_{e*}$ . The gray horizontal dashed line indicates the  $\beta_e = 7kPa$  level, while the vertical one denotes the  $\nu_{e*} = 0.35$  value. Discharges with EHO activity lie in the region inside the red dashed ellipse.

discharges are plotted against of  $\nu_{e*}$ . Here employ the definition  $\beta_e = 2\mu_0 n_e^{\text{ped}} T_e^{\text{ped}} / B_t^2$  (cf. Fig. 10). It is immediate to notice that JET-C discharges have a favourite access to high  $\beta_e$  and low collisionality ( $\nu_{e*} \lesssim 0.35$ ) regions, whereas ILW shots tend to cluster mainly at high collisionality with lower  $\beta_e$  (cf. figure 11). In this space, the set of four discharges given in section II occupies the high  $p_e$ -low  $\nu_{e*}$  region which is well covered by the JET-C ELMy database, contrarily to the ILW shots which barely border it. As mentioned previously, other parameters must therefore play a role in the determination of the quiescent/ELMy state.

Let us first point out that apart from the pedestal height (i.e.  $n_e$ ,  $T_e$  and  $p_e$ ) and collisionality requirements, experiments in DIII-D, ASDEX-U and JT60-U

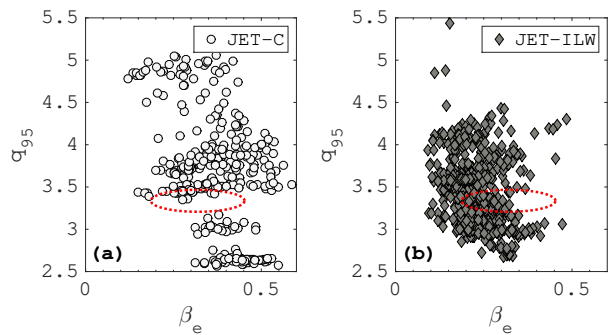


Figure 14.  $q_{95}$  vs pedestal  $\beta_e$  scatter plot of the JET-C (a) and ILW (b) database pulses. The red ellipse has the same meaning as in figure 13.

showed that EHOs are obtained in plasmas with a sufficiently large edge-wall clearance. In DIII-D, ASDEX-U and JET, the plasma-wall gap is enhanced by having large values of triangularity, both upper and lower, whereas JT60 plasmas were able to operate with quiescent phases at low  $\delta$  as long as a sufficient plasma-wall clearance was provided [6]. The necessity of the plasma-wall detachment is found to be a key ingredient for the EHO excitation in analytic modelling [34, 36] which also predicts the dependence upon the value of  $q$  in the pedestal in accordance with numerical simulations of JET-like plasmas [39, 40]. From the experimental point of view, the role of  $q_{95}$  is not as clear, since experiments in DIII-D have been observed to not have preferred values for  $q_{95}$ , whereas ASDEX-U and JT60-U achieved quiescent phases only with a narrow range of  $q_{95}$  [29].

Thus, we identify four parameters that determine the accessibility to the quiescent regime with EHOs:

$$\beta_e, \nu_{e*}, \delta \text{ and } q_{95}. \quad (1)$$

Note that apart from triangularity, all these quantities are local in nature, i.e. they specifically identify the pedestal conditions. We expect that EHOs can be excited if the quantities associated with the database of figure 11 take simultaneously the same values of the ones of the quiescent discharges of section II. Hence, we plot the parameters listed above against each other for the database in of Fig. 11. By assessing the differences between JET-C plasmas with EHOs and the discharges of the JET-C and ILW ELMy database, we can uniquely identify the conditions that have to be met to achieve the quiescent operation regime, and in particular whether such conditions are compatible with metallic wall machines. Since the  $\beta_e - \nu_{e*}$  space has already been analysed in Fig. 13, we plot in figures 14, 15 and 16 the remaining combinations of the parameters given in (1).

By comparing the localisation of Q-EHO shots in the respective parameter space identified by the set of physical variables given in (1), we immediately notice from figures 13-16 that the discharges with EHOs lie at the very boundaries of the respective parameter space. This

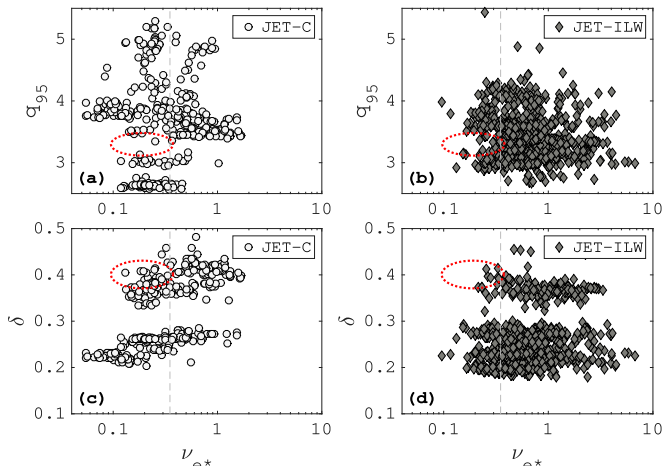


Figure 15. Scatter plot of  $q_{95}$  and  $\delta$  vs pedestal  $\nu_{e*}$  for JET-C ((a) and (c)) and ILW ((b) and (d)) pulses of the ELMy database. The gray vertical line denotes the  $\nu_{e*} = 0.35$  value. The red ellipse has the same meaning as in figure 13. JET-C shots with EHO activity localise at the very edge of the parameter space scanned by the database of Fig. 11.

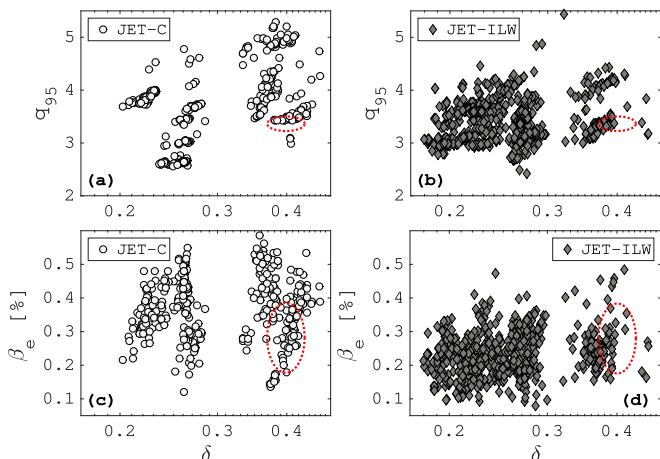


Figure 16. Edge  $q_{95}$  and pedestal  $\beta_e$  vs  $\delta$  scatter plot of the JET-C ((a) and (c)) and ILW ((b) and (d)) database pulses. The red ellipse has the same meaning as in figure 13.

leads us to infer that EHOs have not been observed in the ELMy carbon and ILW database of figure 11 because none of the pedestal parameters had simultaneously the values that are specific to the JET-C quiescent shots of Table I. Noticing further that discharges with similar pedestal features (i.e.  $n_e$ ,  $T_e$  and  $\delta$ ) but different  $q_{95}$  do not exhibit Q-EHO phases, as pointed out in Sec. II we argue that the dependence upon  $q$  is a key ingredient in the mode excitation (see also Ref. [29]) among with the local value of the magnetic shear [37] which is strongly affected by the local bootstrap corrections, and thus collisionality [15, 30–33].

Although EHOs have not been observed in the aforementioned database of ILW discharges, there are some in-

dications from more recent experiments that EHOs might be observed with a metal wall. Indeed, edge magnetic oscillations have been observed, although transiently, in high performance pulses with strong NBI heating. The associated macroscopic parameters, e.g. shaping and pedestal values, are similar to the ones of the quiescent JET-C discharges of table I. Further analyses are however required to have a unique mode identification. Support to the possibility of EHO activity in metallic machines comes from novel ASDEX-U with a metal wall findings, where EHOs have been observed, although transiently, in co-NBI heated pulses with the NBI applied before entering the high confinement phase [41]. Moreover, more recent experimental observations in ASDEX-U reported the presence of EHOs lasting for several hundreds of milliseconds, suggesting the possibility that such oscillations could be steadily sustained [12].

#### IV. CONCLUSIONS

In this work we presented a detailed analysis of quiescent JET discharges exhibiting EHO-type MHD activity. In accordance with previous results on other devices such as DIII-D and ASDEX-U, these oscillations are observed at low collisionality [29] with the pedestal characterised by high temperatures and low density, although densities in JET can be three or four times larger compared to the ones required to sustain EHOs in DIII-D, ASDEX-U and JT60-U. We observed a threshold in the pedestal top plasma density value, beyond which the quiescent phase with EHOs is lost. The density ramp is accompanied by a decrease of the electron temperature, whose pedestal knee also exhibits an inwards shift, so that the associated pedestal collisionality increases. The plasma rotation gradient instead, does not seem to have a significant role in determining the MHD stability against such modes (cf. Fig. 7).

These quiescent discharges have been consequently compared with a database of ELMy shots with both carbon and ITER-like wall conditioning. It is found that the relevant parameters of Q-EHO discharges lie at the very boundaries of the operational space of the ELMy JET-C and ILW pulses of the database. It is worth stressing that EHOs were not observed in the JET-C pulses of the database because the pedestal parameters did not have all simultaneously the specific values characterising the QH discharges. We point out however that some recent JET-ILW pulses exhibit improved performances which may favour the appearance of edge oscillations.

Finally, although more recent work in ASDEX-U [12] seem to point clearly to the possibility that QH regimes with EHOs could be accessible in metallic machines, further analyses are nevertheless required to assess the impact of other parameters, such as  $q_{95}$ , on the MHD dynamics of these scenarios and the steady sustainability of these regimes.

## V. ACKNOWLEDGEMENTS

This work has been carried out within the framework of the EUROfusion Consortium and has received funding from the Euratom research and training programme 2014–2018 and 2019–2020 under Grant agreement No. 633053 and from the RCUK [Grant No. EP/T012250/1].

To obtain further information on the data and models underlying this paper please contact PublicationsManager@ukaea.uk. The views and opinions expressed herein do not necessarily reflect those of the European Commission. This work was supported in part by the Swiss National Science Foundation.

- 
- [1] Leonard A W 2014 *Phys. Plasmas* **21** 090501
  - [2] Viezzer E 2018 *Nucl. Fusion* **58** 115002
  - [3] Burrell K H *et al.* 2001 *Phys. Plasmas* **8** 2153
  - [4] Burrell K H *et al.* 2005 *Phys. Plasmas* **12** 056121
  - [5] Suttrop W *et al.* 2003 *Plasma Phys. Control. Fusion* **45** 1399
  - [6] Oyama N *et al.* 2005 *Nucl. Fusion* **45** 871
  - [7] Solano E *et al.* 2010 *Phys. Rev. Lett.* **104** 185003
  - [8] Nave M F F *et al.* 1997 *Nucl. Fusion* **37** 809
  - [9] Nave G T A *et al.* 1998 *Nucl. Fusion* **38** 179
  - [10] Perez C P *et al.* 2004 *Nucl. Fusion* **44** 609
  - [11] Frassinetti L *et al.* 2021 *Nucl. Fusion* **61** 016001
  - [12] Viezzer E *et al.* 2021 *Progress towards a quiescent, high confinement regime for the all-metal ASDEX Upgrade tokamak, 47th EPS Conf. on Plasma Physics*
  - [13] Groebner R J *et al.* 2001 *Nucl. Fusion* **41** 1789
  - [14] Chen X *et al.* 2016 *Nucl. Fusion* **56** 076011
  - [15] Sauter O *et al.* 1999 *Phys. Plasmas* **6** 2834
  - [16] Sauter O *et al.* 2002 *Phys. Plasmas* **9** 5140
  - [17] Sharapov S E *et al.* 2006 *Nucl. Fusion* **46**
  - [18] Burrell K H *et al.* 2004 *Plasma Phys. Control. Fusion* **46** A165
  - [19] Garofalo A M *et al.* 2011 *Nucl. Fusion* **51** 083018
  - [20] Haskey S R *et al.* 2018 *Plasma Phys. Control. Fusion* **60** 105001
  - [21] Haskey S R *et al.* 2017 *JINST* **12**
  - [22] Kim J *et al.* 1994 *Phys. Rev. Lett.* **72** 2199
  - [23] Liu F *et al.* 2015 *Nucl. Fusion* **55** 113002
  - [24] Hughes J W *et al.* 2018 *Nucl. Fusion* **58** 112003
  - [25] Wagner F 2007 *Plasma Phys. Control. Fusion* **49** B1
  - [26] Sauter O and Medvedev S Y 2013 *Comput. Phys. Commun.* **184** 293
  - [27] Burrell K H *et al.* 2002 *Plasma Phys. Control. Fusion* **44** A253
  - [28] Chen X *et al.* 2017 *Nucl. Fusion* **57** 086008
  - [29] Oyama N *et al.* 2006 *Plasma Phys. Control. Fusion* **48**
  - [30] Saarelma S *et al.* 2013 *Nucl. Fusion* **53** 123012
  - [31] Saarelma S *et al.* 2012 *Nucl. Fusion* **52** 103020
  - [32] Kim S K *et al.* 2020 *Nucl. Fusion* **60** 076022
  - [33] Brunetti D *et al.* 2019 *46th EPS Conf. on Plasma Physics (European Physical Society, Milan, Italy)* paper no P1.1031
  - [34] Brunetti D *et al.* 2018 *Nucl. Fusion* **58** 014002
  - [35] Brunetti D *et al.* 2018 *J. Plasma Phys.* **84** 745840201
  - [36] Brunetti D *et al.* 2019 *Phys. Rev. Lett.* **122** 155003
  - [37] Bustos Ramirez G *et al.* 2021 *Effect of edge magnetic shear on Edge Harmonic Oscillations in plasmas with separatrix, Submitted to Plasma Phys. Control. Fusion*
  - [38] Suttrop W *et al.* 2004 *Plasma Phys. Control. Fusion* **46**
  - [39] Zheng L J *et al.* 2013 *Nucl. Fusion* **53** 063009
  - [40] Zheng L J *et al.* 2013 *Phys. Plasmas* **20** 012501
  - [41] Meyer H *et al.* 2019 *Nucl. Fusion* **59** 112014